Journal of Marine Research, 55, 1103–1126, 1997

A laboratory study of the effects of a sloping side boundary on wind-driven circulation in a homogeneous ocean model

by Ross W. Griffiths[1] and George Veronis[2]

ABSTRACT

A laboratory model is used to investigate the effects of sloping boundaries on homogeneous wind-driven β-plane circulation. The very gentle slopes of real oceanic boundaries raise the possibility that dissipation by lateral diffusion of vorticity to the boundary is largely removed, leaving dissipation only in bottom Ekman layers. The laboratory model is a modification of the rotating 'sliced-cylinder' introduced by Pedlosky and Greenspan (1967) and Beardsley (1969) and in which flow is driven by a differentially rotating lid. The vertical wall is replaced with a side wall having a uniform 45° slope around the entire perimeter. This sloping boundary, like a continental slope, tends to steer the flow along the slope. In the geometry chosen for this study it also provides closed potential vorticity contours through every point in the basin, thus removing the blocked contours of the experiments with a vertical wall and the open contours of ocean basins that approach the equator. For cyclonic forcing there is a northward (Sverdrup) flow in the interior superimposed on a zonal flow so that a particle starts out at the southwest, enters the slope region in the northwest, circles cyclonically along a circle of constant radius (and depth) to a point on the southeast where it crosses constant depth contours and rejoins the original point. The direction of flow is reversed for anticyclonic forcing. The main dissipation of vorticity takes place in the southeast where the flow crosses constant depth contours. For cyclonic forcing the flow is stable and steady under all conditions achieved. For anticyclonic forcing the laboratory flow is unsteady under all conditions attainable and unstable to eddy shedding at sufficiently large Rossby or Reynolds numbers. At large Ekman numbers the onset of instability corresponds to shedding of cyclonic eddies in the region where the boundary current enters the interior, whereas at small Ekman numbers it corresponds to periodic breakup of an anticyclonic gyre in the 'northwest' and the formation of anticyclonic eddies. Eddies of both sign are shed when the forcing is sufficiently supercritical and the Ekman number small. A simple, qualitative argument explains why the cyclonic flow is stable and the anticyclonic flow is unstable when the system is nonlinear.

1. Introduction

Ocean models commonly employ vertical walls and side boundary conditions ranging from slip to no-slip. The choice of side boundary conditions on a vertical wall is found to have a significant influence on the dissipation and therefore on the form of the western boundary current (WBC) and the position at which it separates from the wall (e.g.,

1. Research School of Earth Sciences, The Australian National University, Canberra 0200 ACT, Australia.
2. Department of Geology and Geophysics, Yale University, P.O. Box 208109, New Haven, Connecticut, 06520-8109, U.S.A.

Haidvogel *et al.,* 1992; Dengg, 1993). Yet the real oceans have very gently sloping side boundaries, with slopes of order 1:100 to 1:10. This raises the possibility that most boundary dissipation is in bottom Ekman layers (unless strong stratification isolates the flow from the bottom and there are large horizontal eddy coefficients which allow lateral diffusion faster than Ekman pumping) which may allow the system to equilibrate without dissipation at the sides. In addition, the slopes cause topographic steering of the flow.

Salmon (1992) used the planetary geostrophic equations to study the effects of a continental slope along the western boundary of a basin filled with fluid of constant density and in which the water depth, H, vanishes at the western edge. Boundary currents are confined to the slope region and tend to be steered along the potential vorticity contours, which are inclined only slightly to the isobaths. Thus, the interior flow enters the western boundary layer region above the slope and flows to the southwest corner where it turns westward to cross isobars and then flows northward to exit the boundary layer region. All of the dissipation takes place in the southwest corner rather than along the entire western boundary. In a numerical calculation for a basin with a slope around the entire basin, he confirmed this picture. In a later paper, Becker and Salmon (1997) incorporated the inertial terms to reproduce the same behavior for nonlinear flows and then extended the study to more strongly driven flows. The latter become unstable to eddies generated in the interior region where the fluid flows out of the boundary layer. The present study is a laboratory model of the effects of a sloping bottom variation on the circulation and is thus a laboratory demonstration of the effects considered by Salmon and Becker.

Pedlosky and Greenspan (1967) and Beardsley (1969) investigated homogeneous flow forced by a differentially rotating lid in the 'sliced cylinder' geometry, and these studies have been followed by further experimental, analytical and numerical studies (Beardsley, 1973, 1975; Beardsley and Robbins, 1975; Becker and Page, 1990). The model has been successful in modeling some aspects of the theory of mid-latitude ocean circulation, particularly the interior Sverdrup balance closed by an intense western boundary current.

Recent experimental and numerical studies with the sliced cylinder model have used a much wider basin of smaller aspect ratio H/L, in which the width of the western boundary current is very small compared to the width of the basin (Griffiths and Cornillon, 1994; Griffiths and Kiss, 1997). In these studies, four flow regimes were identified and labeled: quasi-linear, nonlinear and stable, unstable, and chaotic flow. The onset of the eddy-shedding instability for a range of Ekman numbers occurs at a fixed value of a Reynolds number ($Re_\gamma = 123 \pm 4$) based on the velocity and width scales for the $E^{1/3}$ viscous boundary layer. The critical value of Re_γ depends rather weakly on the aspect ratio for $H/L < 0.5$. Thus, when the flow has sufficient inertia, dissipation in the western boundary current does not suffice to balance the forcing in the interior of the basin and eddy shedding is required in the adjustment from the separated jet to the broad interior flow. The interior flow, however, remains a slow meridional drift as given by a Sverdrup balance, and the experimentally determined mean streamlines are consistent with those computed by Beardsley (1973) and by the quasi-geostrophic code of Becker and Page (1990).

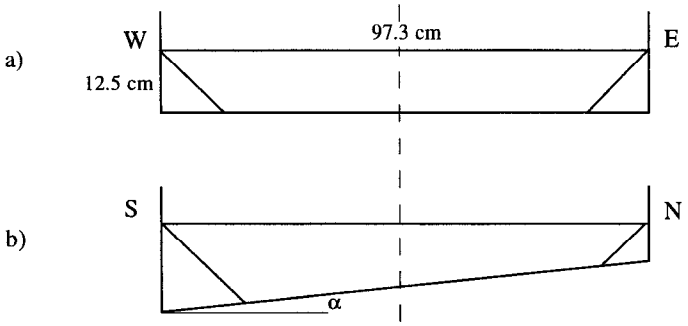

Figure 1. Sections illustrating the experimental basin geometry across (a) east-west and (b) north-south diameters (not to scale).

Here we report the results of experiments with a modified version of the wide 'sliced-cylinder' apparatus of Griffiths and Kiss (1997), in which the vertical wall is replaced by a uniformly sloping boundary such that the water depth vanishes at the edge of the basin. In the interior of the basin we retain the planar bottom with a small slope in order to make use of the topographic analogy to the planetary β-effect.

In an earlier version of this manuscript we had included an analytical treatment of the linear case. However, a referee questioned one of the details in the results of the analysis so we have deleted that section in order to meet the time schedule for the Welander issue. The analysis will appear later.

2. Apparatus

The experiments were carried out in a rotating circular tank of diameter L, nominally 1.0 m, fitted with an internal planar base and a differentially rotating lid. The base slope, α, relative to the horizontal was set at $\tan \alpha = 0.10$ and provided a 'north-south' gradient of potential vorticity f/H, where $f = 2\Omega$ is the (uniform) Coriolis parameter. The rotating planar lid fitted inside the walls of the circular tank and could be fixed at the desired height above the base. A 0.1 cm gap around the perimeter of the lid was sealed by a sliding nylon sleeve arrangement. The lid was supported and driven by eight equally spaced vertical strutts bolted to a 1.1 m diameter drive ring and connected to a bearing assembly rigidly mounted above the tank. In these experiments the lid was rotated in a horizontal plane by a stepper motor with a drive wheel acting on the outer rim of the drive ring. The lid could be rotated relative to the tank either clockwise or anticlockwise at a wide range of speeds. The total mean depth of water, H_O (the depth at the center of the tank), was 12.5 cm and the working diameter was 97.3 cm. Hence, the aspect ratio H_O/L is 0.128, much smaller than the aspect ratios used by either Beardsley (1969) ($H_O/L = 0.502$) or Becker and Page (1990) ($H_O/L = 1.17$).

The sloping side boundary was part of a simple 45° cone with its axis coincident with the vertical axis of the tank (Figs. 1, 2). The cone was made from a single plastic sheet 3 mm

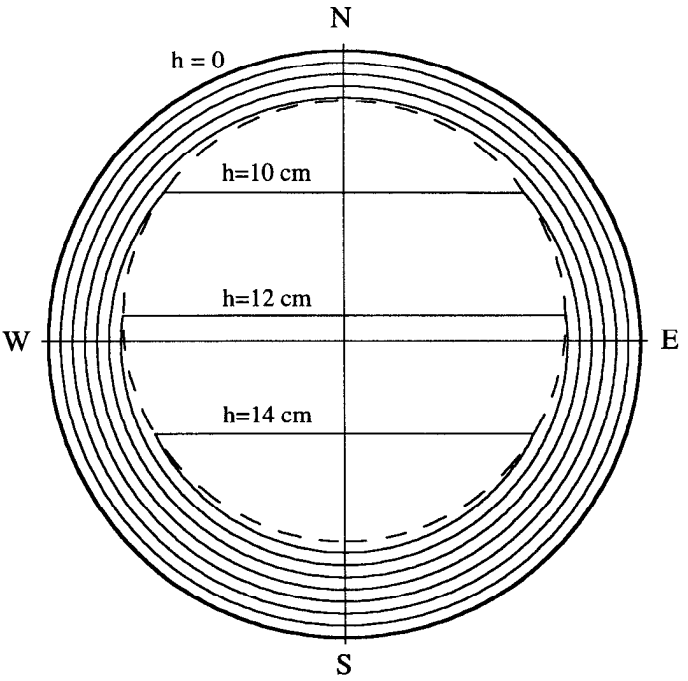

Figure 2. Plan-view of the basin with depth contours every 2 cm of depth. The broken line shows the intersection of the interior bottom (a plane with slope 1:10) and the sloping boundary (a cone with slope 45°). The 8 cm depth contour is slightly outside the circular contour that divides the circular contours from the D-shaped contours.

thick and cut to the required shape before being wrapped and joined. The top of the cone intersected the vertical sides of the tank at the base of the lid. The working fluid beneath the lid therefore occupied a circular basin of radius $a = 48.65$ cm. The curve (shown dashed in Fig. 2) at which the bottom of the conic section met the sloping base is an ellipse given by

$$r_i = (a - H_O/\tan\theta)/(1 - \tan\alpha \sin\phi/\tan\theta), \tag{2.1}$$

where r_i is the radius from the axis of the tank, ϕ is the azimuthal coordinate (measured anticlockwise with $\phi = 0$ at 'east'), and $\tan\theta$ (= 1) is the side wall slope. The circle tangent to the ellipse at the northern limit will be referred to as the limiting circle. The top of the sloping boundary was sealed against the vertical tank wall using a rubber gasket and the bottom was sealed against the base using a silicone sealant. The base and sloping wall were white in order to facilitate flow visualization from above.

As a result of the interior bottom slope, the width of the sloping boundary varied with azimuthal position. Contours of constant water depth were closed concentric circles for radii $r > r^* = 40.17$ cm. Elsewhere in the tank constant depth contours were D-shaped paths consisting of a circular arc over the conic boundary around the deepest ('equatorward') region and closed by a straight 'east-west' line across the interior of the tank (e.g.,

the 10, 12, and 14 cm depth contours in Fig. 2). In contrast to the sliced-cylinder model with vertical walls, in which there are no closed geostrophic contours, this arrangement has *only* closed geostrophic contours. Apart from some dissipation in the outer wedge-shaped corner, where the water depth vanishes, generation and dissipation of vorticity can occur only through Ekman layers on the lid, on the bottom of the interior of the basin and on the conical sloping bottom.

In the remainder of this paper we shall freely use (northern hemisphere) geographic terms to indicate the various positions and directions of motion in this β-plane analog. Thus 'north' refers to the shallowest end of the tank, and 'east' is to the right of north.

3. Detailed description of experimental procedures

In attempting experiments with extremely slow forcing, it was found that small temperature differences due to heat exchange with the room could generate small-scale vertical convection. Hence temperature control was necessary. This was achieved by placing 5 to 10 cm of water above the lid and pumping this water through a heat exchanger in a constant temperature bath. The same water was also pumped through side chambers between the cylindrical tank and a large square box that surrounded the whole tank (the outer box is a standard arrangement normally used to allow side viewing of flows in the circular tank without the optical distortion of a cylindrical wall, though the additional sloping boundary prohibited side viewing in this case). The water in the working chamber was maintained at 20.9 ± 0.3°C.

Tank rotation speeds $\Omega = 0.5$ to 3.0 rad s^{-1} and relative lid speeds $\Delta\Omega = 0.004$ to 0.18 rad s^{-1} (periods 1440 s to 35 s) were used to give Rossby numbers $Ro = \Delta\Omega/\Omega$ from 0.002 to 0.18 and Ekman numbers $E = \nu/\Omega H_O^2$ from 2.1×10^{-5} to 1.3×10^{-4}, for kinematic viscosity $\nu = 1.0 \times 10^{-2}$ cm^2 s^{-1}. For anticyclonic forcing the bulk of the flow along the sloping boundary follows paths of constant depth. The parameters used give $E^{1/4} \sim \tan\alpha$, conditions under which the frictional, western boundary current in a basin with vertical walls is predicted by Beardsley (1969, 1975) to be in a mixed regime between that of Stommel (1948) (dominated by Ekman dissipation) and that of Munk (1950) (dominated by lateral diffusion and dissipation on the side wall). Use of smaller base slopes would have produced wider boundary currents. We also aimed to keep the boundary current width smaller than the width of the slope region so that the effect of the slope could be most easily determined. Similarly, much smaller Ekman numbers could not be achieved without using much greater water depths and, therefore, larger aspect ratios.

Effective flow visualization and measurement in these experiments was achieved in the same manner as in the case of a vertical wall (Griffiths and Cornillon, 1994; Griffiths and Kiss, 1997). Narrow streams of neutrally-buoyant dye were bled slowly into the flow at a number of strategic locations from 1 mm diameter stainless steel syringe tubes passing through the base and slope. These outlets were positioned along an east-west line through the axis of the tank and connected, through the space under the sloping base, to control needle valves and reservoirs above the tank. The most effective positions for these passive

tracer outlets were found to be over the western and eastern slopes. From these points dyed streamlines passed along the slope and across the interior. In the majority of runs the system was rotated anticlockwise and outlets were positioned at the 'west' ($\phi = \pi$) at the radii: $r = 437$ mm (over the upper slope); $r = r^* = 402$ mm (on the limiting circle); $r = 382$ mm (over the lower slope); $r = r_i(\phi = \pi) = 361$ mm (directly above the slope-base intersection), and at $r = 344$, 287 and 0 mm (several points across the interior). A further tracer stream was released above the slope-base intersection at $\phi = 0$. In initial experiments, tracers on streamlines at different depths (2 cm from the lid and 2 cm from the base) indicated no discernible depth-dependence to the flow. Thus in the majority of runs the outlets were placed at the local mid-depth in the water column. In a few runs the system was rotated clockwise with the dye outlets left in the same positions so that they were then in the east.

The tracer density was carefully adjusted to match that of the water by adding a very small quantity of salt (0.78 g/l) to the water and precisely adjusting each color of dye solution to a perfect match (to within 0.002%). There were some unavoidable effects of double-diffusive convection due to differences in the solution compositions, causing the narrow dye streams eventually to become more like vertical sheets, with some slow lateral dispersion. However, the released dye was otherwise passively advected with the flow to reveal the streamlines (where the flow was steady), eddy shedding and the patterns of mean flow when the flow was unsteady. Velocities were measured from time-lapse video records of tracer positions by tracking the positions of the leading end, of short spaces inserted in the streams and of easily recognizable features in the patterns of dye produced by the flow. Passive dye tracer enabled us to measure very small speeds in the interior flow (10^{-2} cm s^{-1}) and relatively large speeds in the boundary current and eddies (1 cm s^{-1}), and avoided difficulties encountered in keeping sufficient particulate tracers in suspension within the laminar flow for many hours. The flow visualization was recorded on still film and time-lapse video tapes (with speed-up factors from 8 to 80).

4. Results for cyclonic forcing

a. Streamlines. The photographs in Figure 3 illustrate the patterns of tracer advection observed in experiments with cyclonic forcing once dye has been carried around a full circuit of the basin. The flow is steady and the dye indicates streamlines. Equivalent experiments in the same apparatus but with a vertical side wall (Griffiths and Kiss, 1997), showed a rapid southward flowing current near the western (left) side of the tank and a much slower, northward flow throughout most of the interior of the basin. That flow is consistent with Stommel's (1948) westward intensified circulation. With the sloping boundary of the present experiment the flow on the upper slope is counterclockwise along circles of constant depth (or f/H). Closer to the interior where the curves of constant depth are the D-shaped contours described earlier, the flow on the western side is slightly enhanced and that on the eastern side is northward and somewhat weaker. Figure 4 shows the difference at $y = 0$ (but this different behavior between east and west on the lower slope

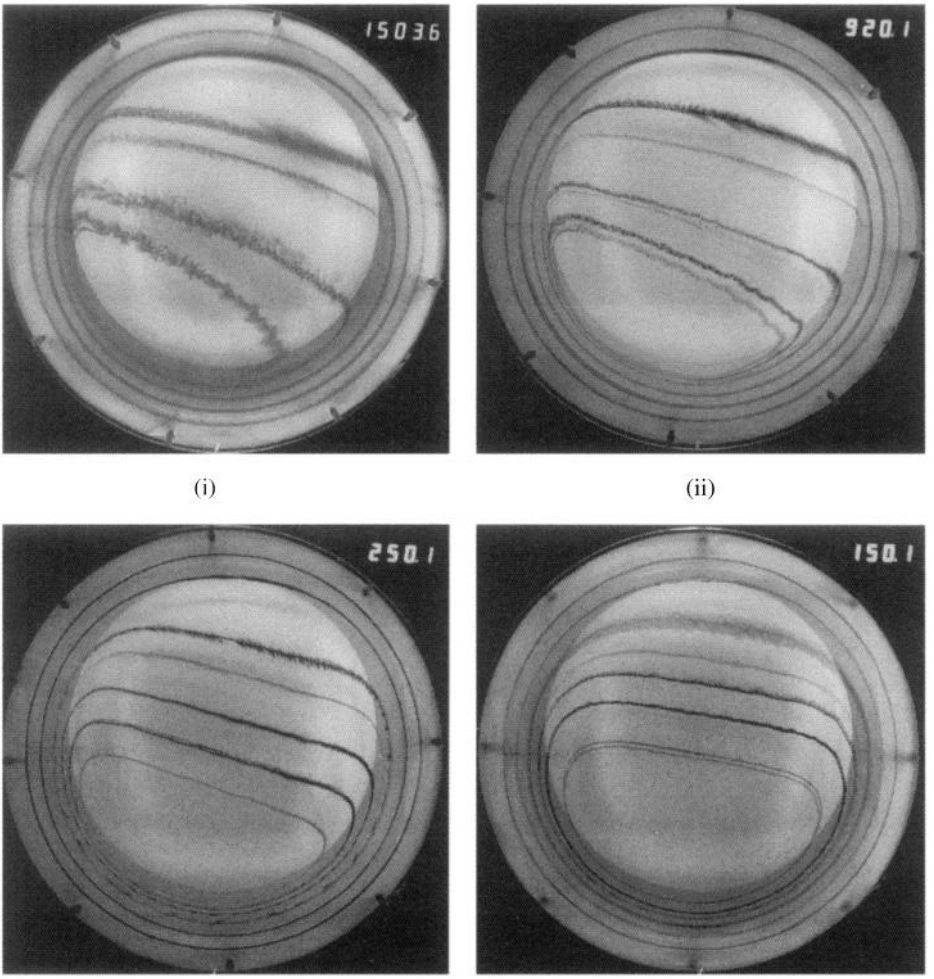

Figure 3. Photographs of the streamlines revealed by advection of dye in the steady flow produced by cyclonic forcing for four different forcing strengths. In each of these runs $\Omega = 2.000$ rad s^{-1} counterclockwise and $E = 3.15 \times 10^{-5}$. (i) lid period 759.7 s, $Ro = 0.0041$; (ii) lid period 372 s, $Ro = 0.0084$; (iii) lid period 88 s, $Ro = .0357$; (iv) lid period 34 s, $Ro = 0.0924$. The numbers in the corner of each frame show the time (in table rotation periods) elapsed since the dye was started. In the interior the water shallows toward the top of the image, referred to as 'north.' A small allowance must be made for parallax errors due to the location of the camera on the axis of the tank and 2 m above the lid. These photographs were taken after dye from each outlet had been advected around at least a full circuit of the basin, in some cases several circuits, leading to the fuzziness of the dye streams.

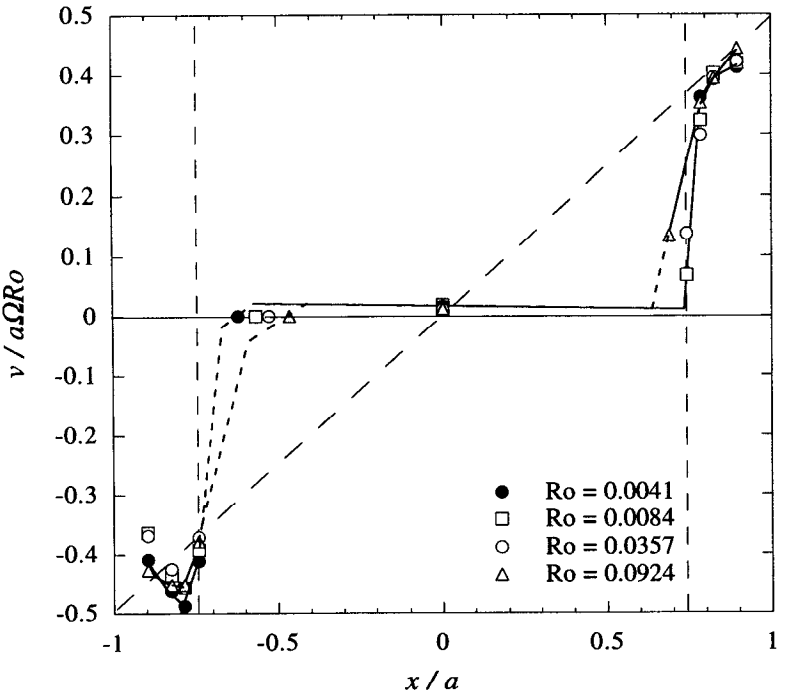

Figure 4. Measurements of the northward component of normalized velocity across the line $y = 0$ for cyclonic forcing with $E = 3.1 \times 10^{-5}$ and four values of Ro. The position in x is plotted as the distance from the center of the tank normalized by the tank radius a. The diagonal broken line is the arbitrary reference solid-body profile $v = 0.5\Delta\Omega r$. The vertical broken lines indicate the edge of the sloping boundary at east and west.

is valid at all values of y). With a sloping boundary the flow in the interior is no longer predominantly toward the north but rather toward the west-north-west. Particles of fluid enter the interior on the eastern side and flow northward and westward into the slope region on the western side. The flow on the lower slope is along circles of constant depth counterclockwise from northwest to southeast but with the help of friction it crosses constant depth contours just before it enters the interior on the eastern side. Thus, the region of frictional dissipation is not on the west, as it is in Stommel's ocean model, but rather on the eastern side where the flow crosses depth contours from shallow to deep water.

Each dye stream formed a circuit of the basin which was closed to within the precision of our observations (±2 mm) and the width of the stream (usually ~2 mm after passing around one circuit). On its second circuit the dye followed the same path again around the basin. The precision of the closing of the circuit was particularly marked over the upper slope, where dye streams returned so exactly to the source syringe tube that they were seen to divert around both sides of the vertical tube. Streams crossing the interior were also closed, but several factors (local broadening of the streams as they pass from the fast flow

of the slope to the very slow flow of the interior, gravitational (double diffusive) instability and the angle of the camera's view of the vertical sheet of dye from the axis of the tank) caused these streams to appear somewhat smeared in their second circuit. The photographs in Figure 3 show the smeared streams and the overlapping of two or more circuits when the dye release was continued. We also noted that the dye tracer on the nearly circular streamlines over the upper slope persisted as fine vertical sheets for an indefinite time (longer than several hours) after the dye source was turned off. Since these times were much greater than the Ekman pumping time scale (~30 s) for that depth, we conclude that the dye was continuously pumped into the Ekman layer near the lid (where it became too stretched to be visible), carried out to the rim of the basin and then returned to its original radius through the bottom Ekman layer. There was certainly no net radial flux of water across this radius. In the interior, dye streams in their second cycle of the basin could sometimes be seen by eye to be concentrated at a depth different from their first cycle. However, side views and accurate measurements of the vertical level of the dye were not possible due to the opaque sloping boundary.

Another difference from the vertical wall case was the absence of a narrow viscous boundary current in the east, traveling in the same direction as the boundary current in the west. This was replaced by the strong (nearly circular) anticlockwise flow along the slope. Over the lower slope the flow turned to pass off the slope in the east into the deeper water of the interior; there was no detectable overshoot in the form of a looping motion (as there is for anticyclonic forcing and also for the vertical wall case), even at the largest Rossby numbers used. Similarly, the interior streamlines merged smoothly with the flow over the lower slope in the west. In some runs we stopped the lid forcing once the dye had marked streamlines around a full circuit of the basin and observed that the dye lines remained unchanged as the flow came to a halt, apart from a sharpening of the corners where straight lines across the interior met circular paths over the slope.

b. Structure of the boundary current. Profiles of northward velocity across the line $y = 0$ are shown in Figure 4 for four runs having the same Ekman number but Rossby numbers covering a wide range. They reveal that the azimuthal flow is intensified on the western side. In the east, the velocity on the upper slope approaches, as a point of comparison, the simple solid body profile $v = 0.5\Delta\Omega r$. Over the lower slope, where the water is shared with the interior, the velocity falls farther toward the relatively slow north-south velocities of the interior. At the west the velocity over the lower slope is substantially greater than in the east, but decreases toward the solid body profile over the upper slope (although there are limited data in that region). In the interior of the basin there is a slow northward (and westward) drift. Volume is conserved in these measurements, since the integrated northward transport in the east and interior match the southward flux in the west.

The maximum velocity over the slope in both the east and west, normalized by $\Delta\Omega a = a\Delta Ro$ (Fig. 4), is independent of the Rossby number to within the scatter of the data. The only dependence on Rossby number appears to occur off the edge of the slope in the west,

where the boundary current width (as measured by the radius of zero velocity) is greater for larger Rossby numbers. Runs having different Ekman numbers reveal a dependence on E; this will be discussed in Section 5 in the context of anticyclonic forcing.

c. Interior velocities. The northward component of velocity v measured along the east-west section $x = 0$, again normalized by $\Delta\Omega a = a\Omega Ro$, is plotted as a function of the latitude y in Figure 5a. The data show that v is directly proportional to the Rossby number and independent of the latitude (although there may be a small decrease in v northward):

$$v = (0.0138 \pm 0.0003)\, a\Omega Ro. \tag{4.1}$$

In Figure 5b the corresponding normalized values of the eastward component of velocity u across the same section $x = 0$ are shown as a function of y. This component too is directly proportional to Ro (except for the run at a very large Rossby number), but decreases linearly with y toward the northern side of the basin:

$$u = -(0.043 + 0.033\, y/a)\, a\Omega Ro. \tag{4.2}$$

The zonal velocity is three to four times greater than the northward component, reflecting the orientation of streamlines in the interior. The dependence of velocity on x was not measured in detail. However, with v essentially constant with y and the slightly convex shape of the streamlines, it is clear that u increases in magnitude as x decreases.

5. Anticyclonic forcing

a. Streamlines. When the direction of lid motion was reversed and when the forcing was weak, the pattern of flow was close to that for the cyclonic case but with the velocities reversed. However, there was now a clear Rossby number-dependence to the streamlines. Photographs of the dye streams for six anticyclonic cases are shown in Figure 6a. In this case the dye tracers released over the slope at the west were advected northward. The streamline over the *upper* slope passed around the basin with only small variations in azimuthal velocity and small deviations from constant radius. The most noticeable deviation occurred for larger Rossby numbers and was in the northern part of the basin; the motion along the streamline slowed as it approached the north and the stream was suddenly diverted to larger radii. The next dye stream, released at the radius of the circle dividing circular and D-shaped depth contours, remained at its source radius around the entire circuit of the basin for very small Rossby numbers. For larger Rossby numbers it appeared to meet a stagnation point close to the shallowest point of the interior (north), around which it had to pass by deviating to smaller radii, hence entering and crossing the interior. This is in contrast to flow with a vertical wall, in which the stagnation point occurs on the wall at 35° west of north (and corresponds to separation of the boundary current, Griffiths and Kiss, 1997).

Under most conditions the dye stream released above the edge of the slope at the west was carried well to the north before leaving the slope, a path which takes the stream far

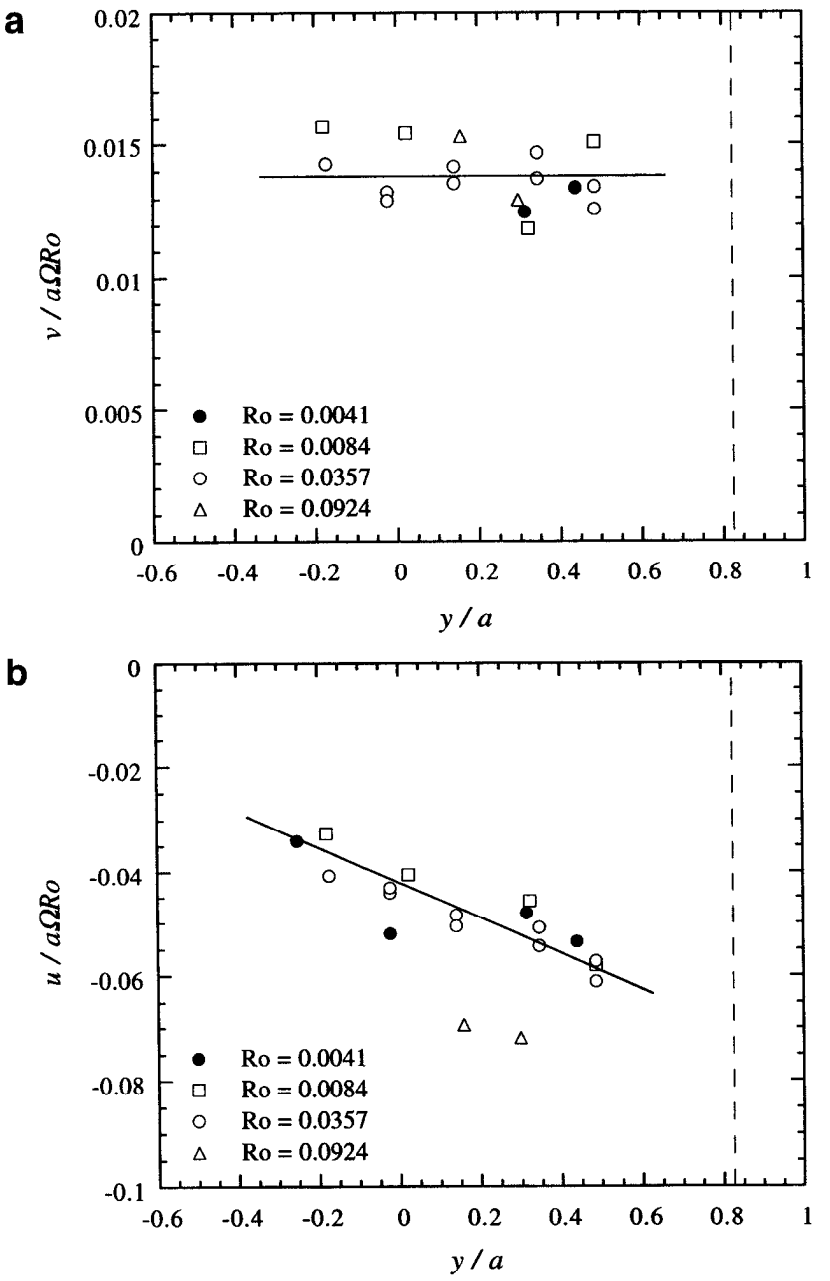

Figure 5. Measurements of the normalized interior velocity components (a) v northward and (b) u eastward for cyclonic forcing as functions of the north-south position y/a along the line $x = 0$. The vertical broken line indicates the position $y/a = 0.83$ of the edge of the slope at the north.

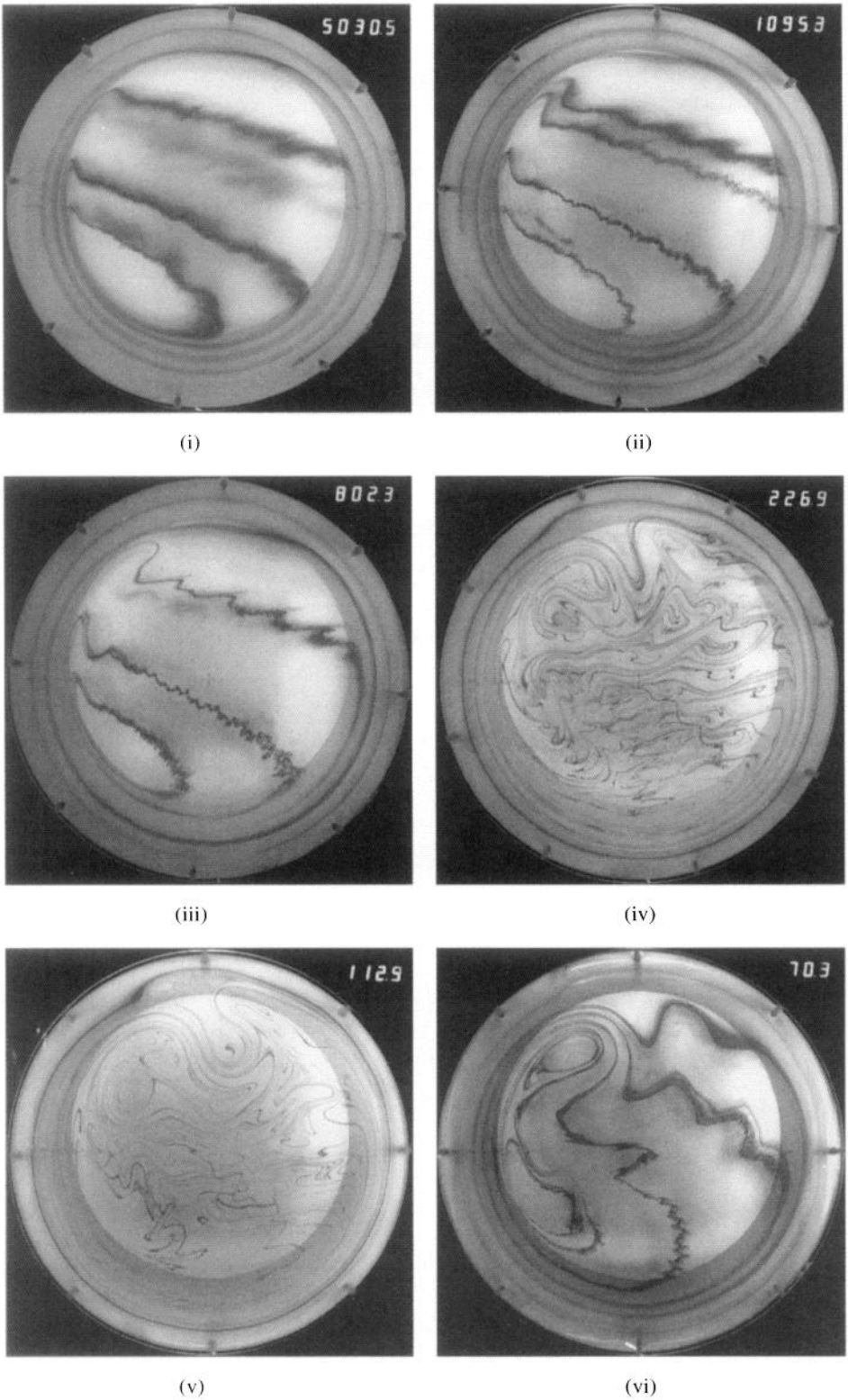

(i) (ii)

(iii) (iv)

(v) (vi)

Figure 6a.

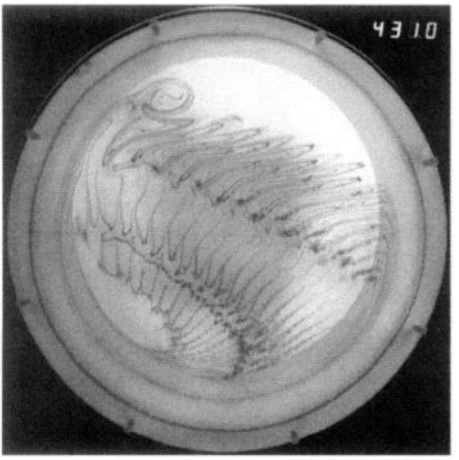

(i)

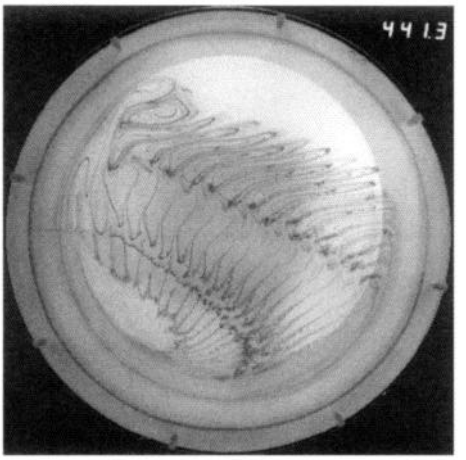

(ii)

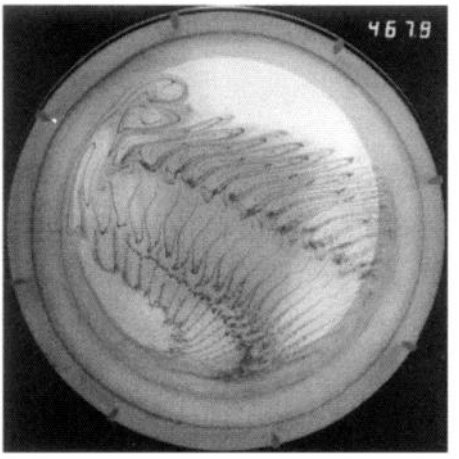

(iii)

Figure 6b.

Figure 6. (a) Photographs of the paths of dye in the flow produced by anticyclonic lid motion. For the runs in (i) to (v) $\Omega = 2.000\ \mathrm{s}^{-1}$ counter-clockwise and $E = 3.15 \times 10^{-5}$; (i) lid period 734 s, $Ro = 0.0043$; (ii) lid period 317 s, $Ro = 0.0099$; (iii) lid period 207 s, $Ro = 0.0151$; (iv) lid period 61 s, $Ro = 0.052$; (v) lid period 40.8 s, $Ro = 0.077$. The run in (vi) had a larger Ekman number: (iv) $\Omega = 1.000\ \mathrm{s}^{-1}$, $E = 6.3 \times 10^{-5}$, lid period 110 s, $Ro = 0.057$. These photographs were taken after dye from each outlet had been advected around a full circuit or more. (b) Photographs showing three stags during a cycle of anticyclonic eddy shedding due to break-up of the anticyclonic gyre in the northwest. $W = 2.000\ \mathrm{s}^{-1}$ counterclockwise, lid period 151.6 s, $E = 3.15 \times 10^{-5}$, $Ro = 0.0207$. The dye outlet at mid-slope at west was not used in this run. All dye streams undergo large north-south fluctuations outside the slope region.

from the depth contour extending east from the source. After leaving the slope, this stream looped back to deeper water (lower latitude) before crossing the interior. Under sufficiently strong forcing, eddies were sometimes formed in this stream in a manner similar to that reported for the vertical wall basin (Beardsley, 1969, 1973; Beardsley and Robbins, 1975; Griffiths and Kiss, 1997). In these cases cyclonic eddies formed where the rapid outflow from the boundary current turned left away from its path around a permanent anticyclonic recirculating gyre to flow instead in a southeastward direction across the interior. However, in other runs instability of a different kind involved a breakup of the anticyclonic gyre and periodic shedding of anticyclonic eddies. Three stages during a cycle of anticyclonic eddy formation in such a case are shown in Figure 6b. For sufficiently strong forcing and small Ekman number, some conditions gave rise to eddies of both sign. In all cases eddy shedding led to stirring of passive tracer across mean streamlines. However, the extent of the stirring was significantly less extensive with the sloping wall than it was with a vertical wall.

Apart from the occurrence of instability, another contrast with the cyclonic case was that anticyclonic forcing did not give rise to a completely steady flow. Even at Rossby numbers as small as 2×10^{-3}, at which the flow was expected to be close to linear (since $Ro \approx 0.002 < E^{1/2}$), unsteadiness was evident as an oscillation in the small loop in the northwest. The amplitude of both the loop and the oscillation in the northwest increased with Rossby number. Similar observations were reported for a vertical side wall (Griffiths and Kiss, 1997). We conclude that for a truly linear regime to be attained, Rossby numbers less than 10^{-3} would have been required.

For the weakest forcing there was a single large anticyclonic gyre centered in the southwest. Flow from the western slope into the interior was distributed over all latitudes $y > -0.7a$. For strong forcing there were two anticyclonic gyres, the one in the southwest and a smaller and more unsteady gyre in the northwest. Much of the outflow from the slope under these conditions was confined to a loop current at latitudes north of $y = 0.6a$ (35° west of north), but some outflow from the slope region persisted at latitudes between the two gyres (near $y = 0$ to $0.3a$). Under these conditions the dye stream released over the edge of the slope entered the interior at a latitude that oscillated in response to the eddy shedding from between the two gyres to the loop around the north of the northwestern gyre.

Mean streamlines in the interior were again at an angle to the depth contours. The angle was larger for larger Ekman numbers, causing streamlines to be oriented more north-south than under cyclonic forcing. In the east, where the streamlines met the slope, water columns moved up the slope and turned right to circle relatively rapidly along a constant radius around the southern part of the basin back to their starting points.

b. Instability. Each run with anticyclonic forcing was classified as stable or unstable (to eddy shedding) and the results plotted in (Ro, E) space (Fig. 7a). We also distinguished between the two forms of eddy shedding at marginally unstable conditions: a periodic shedding of cyclonic eddies from the diverging outflow as it merges into the steady flow

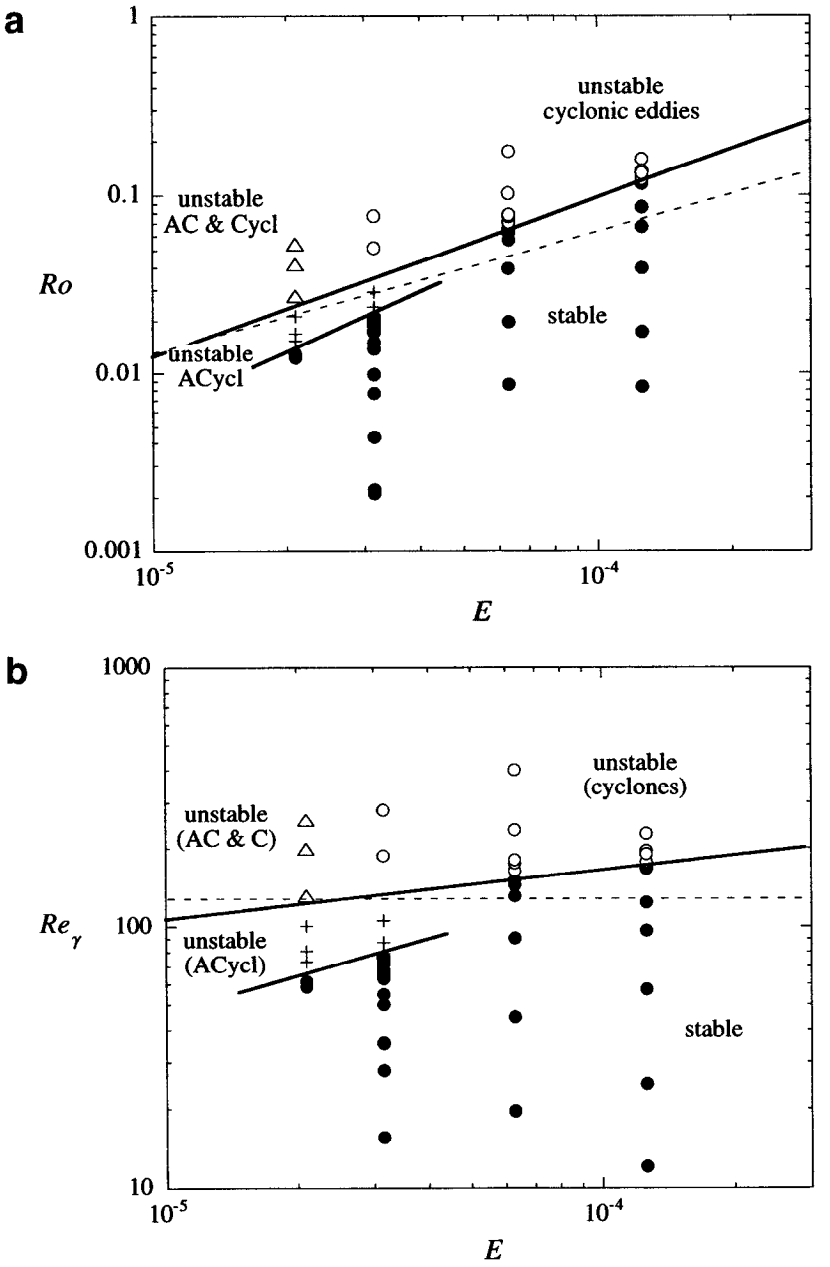

Figure 7. Flow regimes under anticyclonic forcing. Each run is plotted in parameter space and classified as stable, unstable with only cyclonic eddies, unstable with only anticyclonic eddies, or unstable with eddies of both signs. In (a) the runs are located in terms of the external variables (Ro, E) whereas in (b) they are plotted in terms of (Re_γ, E). The solid lines are inferred boundaries between the regimes; the broken line is the stability boundary for shedding of cyclonic eddies found in corresponding experiments with a vertical side wall.

across the interior (this is the type of instability observed to occur first in the case of a vertical wall), or a periodic formation of anticyclonic eddies due to breakup of the anticyclonic gyre within the northern loop. From Figure 7a it can be seen that the onset of instability took the form of shedding of cyclonic eddies only at $E > 5 \times 10^{-5}$. At smaller Ekman numbers the first instability is the shedding of anticyclonic eddies. At the smallest Ekman number sufficiently strong forcing gave rise to instability through both mechanisms and eddies of both sign were shed. Thus the regime diagram shows that the formation of cyclonic eddies replaced the formation of anticyclones at an intermediate value of E. However, the critical Rossby number Ro_c for onset of cyclonic eddy shedding is well described by a single power law curve over the full range of E:

$$Ro_c = 338\, E^{0.89}. \tag{5.1}$$

For $E < 5 \times 10^{-5}$ the onset of instability occurred through anticyclonic eddy shedding at the smaller Rossby number Ro_a, where

$$Ro_a = 5.7 \times 10^5\, E^{1.6}, \qquad E < 5 \times 10^{-5}. \tag{5.2}$$

The onset of cyclonic eddy shedding occurs at conditions very similar to the critical conditions reported for the vertical wall case (broken line on Fig. 7), although the variation with E is slightly greater with the sloping boundary. Thus the sloping boundary and the resulting anticyclonic eddy shedding extend the range of unstable conditions in the present system to smaller Rossby numbers for small Ekman numbers. The anticyclonic eddies represent a greater unsteadiness of the anticyclonic northern loop in the northwest.

Instability in the sliced-cylinder with a vertical wall was found to occur at a fixed critical value of a Reynolds number Re_γ, defined in terms of the boundary current velocity scale $U = \Delta\Omega a$ and the width scale $\gamma = H\,(E/2\tan\alpha)^{1/3}$ of a purely viscous (lateral) boundary layer (Griffiths and Kiss, 1997). The parameter becomes (omitting a factor of $2^{-4/3}$ on the right-hand side)

$$Re_\gamma = U\gamma/\nu = Ro\, E^{-2/3}(L/H)\,(\tan\alpha)^{1/3}. \tag{5.3}$$

The critical value of this Reynolds number, $Re_\gamma = 123 \pm 4$, was independent of basin aspect ratio and Ekman number, whereas the critical values of a number of alternative Reynolds numbers depended on the other parameters. In Figure 7b we replot the classifications from Figure 7a in terms of Re_γ and find that for the present system the critical value for cyclonic eddy shedding: $Re_\gamma = 160 \pm 9$ for $E > 5 \times 10^{-5}$. There is a weak dependence on the Ekman number which is enhanced by the breakup of the anticyclonic gyre at small Ekman numbers, leading to instability at values of Re_γ as small as 70.

c. The boundary current. Profiles of the northward velocity component v across the section $y = 0$ for runs having similar cyclonic Rossby numbers but a range of Ekman numbers are shown on Figure 8. The data reveal an Ekman number dependence with maximum speeds in the boundary current over the lower slope being slightly larger for larger E. The data also

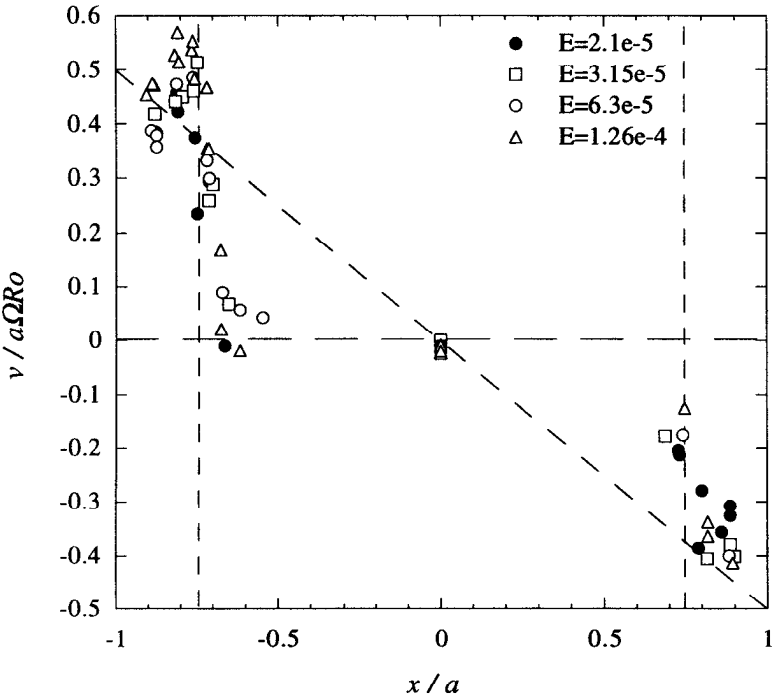

Figure 8. Measured profile of the northward component of (normalized) velocity across the line $y = 0$ for anticyclonic lid motion and similar Rossby numbers $0.01 < Ro < 0.02$. The northward flowing boundary current at the west appears as velocities lying above the dashed diagonal line, which is the arbitrary solid-body reference profile. Vertical dashed lines indicate the edge of the sloping boundary. The nearly horizontal dotted line at small negative velocities indicates the interior flow, which was measured explicitly only around $x = 0$ and near the slope.

provide some evidence that the boundary current flow may extend slightly farther off the slope for larger Ekman numbers. The solid body profile $v = 0.5\Omega r$ again provides a convenient, albeit arbitrary, reference against which to see the east-west asymmetry and make comparison to the data for cyclonic forcing (Fig. 4). As with cyclonic forcing, the speeds on the upper slope at both east and west decrease to (or even below) this solid body reference.

d. Interior velocities. The northward component of velocity v was again measured along the line $x = 0$ and is plotted in Figure 9a as a function of the latitude y for four runs having the same Ekman number but different Rossby numbers. These measurement were not taken in the deepest region of the basin, where the streamlines tended to curve around from the southeastward interior flow to the westward flow on the slope, so that u vanished. At locations very close to the slope at the north the interior velocity was large and tended toward the purely eastward flow on the slope. Apart from this internal boundary layer

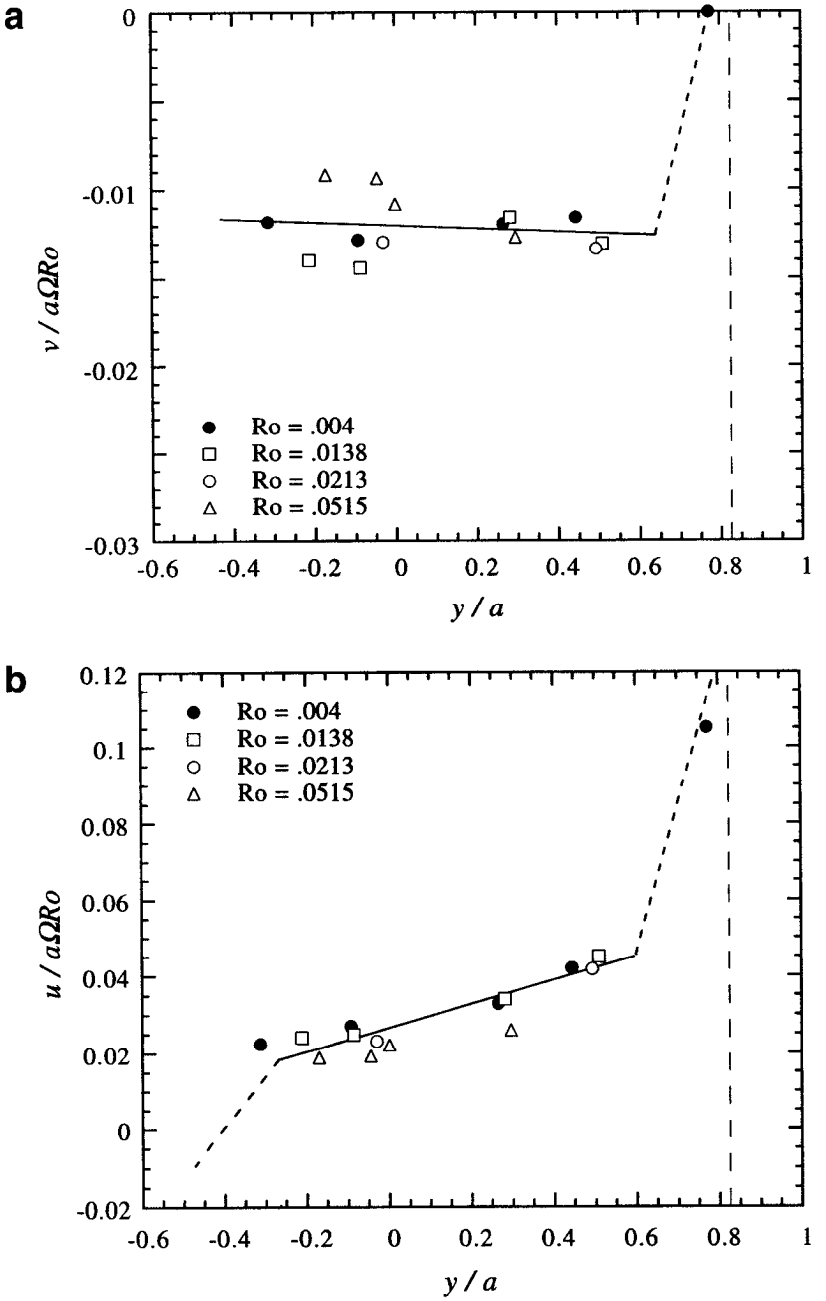

Figure 9. Normalized components of the velocity along and across the center line $x = 0$ in the interior for anticyclonic forcing as functions of the latitude y/a for four runs having a fixed value of $E = 3.15 \times 10^{-5}$ and various values of Ro: (a) northward component v, (b) eastward component u. The vertical dashed line indicates the position of the edge of the slope, the solid straight lines are the best fits by linear regression.

region, and as with cyclonic forcing, v showed no significant dependence on the latitude and was directly proportional to the Rossby number:

$$v = -(0.0121 \pm 0.0004)\, a\Omega Ro, \qquad E = 3.15 \times 10^{-5}. \tag{5.4}$$

The eastward component u, plotted in normalized form in Figure 9b, increased northward. In normalized form it showed only a very weak dependence of Rossby number and to a good approximation:

$$u = (0.026 + 0.031 y/a)\, a\Omega Ro, \qquad E = 3.15 \times 10^{-5}. \tag{5.5}$$

Similar measurements were made for a series of runs having similar Rossby numbers but different Ekman numbers (Fig. 10a,b). The normalized velocity components for each run remained consistent with a northward velocity that is independent of latitude and a u-component that increased northward. However, v was smaller for larger Ekman number while u was independent of E. Fitting a straight line to the data on Figure 10b gives the same result as (5.5).

In order to characterize the dependence of the interior velocity on external parameters we interpolated the data on Figures 9 and 10, using a straight line of best fit, and evaluated the components $u(0,0)$ and $v(0,0)$ at the axis of the basin for each run. A plot of the normalized velocities at the axis as functions of the Ekman number (Fig. 11) confirms the result that $u(0,0)$ is independent of E:

$$u(0,0) = (0.025 \pm .003)\, a\Omega Ro \tag{5.6}$$

whereas $v(0,0)$ varies in a manner consistent with $E^{1/2}$:

$$v(0,0) = -(2.6 \pm 0.3)\, a\Omega Ro E^{1/2}. \tag{5.7}$$

As a further demonstration of the Rossby number dependence we plot in Figure 12a the normalized values of $u(0,0)$ as a function of Ro and in Figure 12b the values of $v(0,0)/(a\Omega Ro E^{1/2})$ as a function of Ro. For u there is again no dependence on E, and the uncertainties on each data point make the small decrease with increasing Rossby number noted above barely significant. This variation might be a result of the changing dynamics of the eddy-shedding instability. For the north-south component there is no systematic trend with Ro. Two of the most nonlinear runs gave slightly smaller values for v, but the differences are within the uncertainties of the data.

6. Discussion and conclusions

A simple physical argument can be put forth for the behavior of the system when the flow is linear. For cyclonic driving a column of fluid that has a large depth in the eastern interior near the ellipse is forced northward by the rotating lid, becoming shorter as it moves northward. This flow in the interior corresponds to the Sverdrup flow in the oceanic

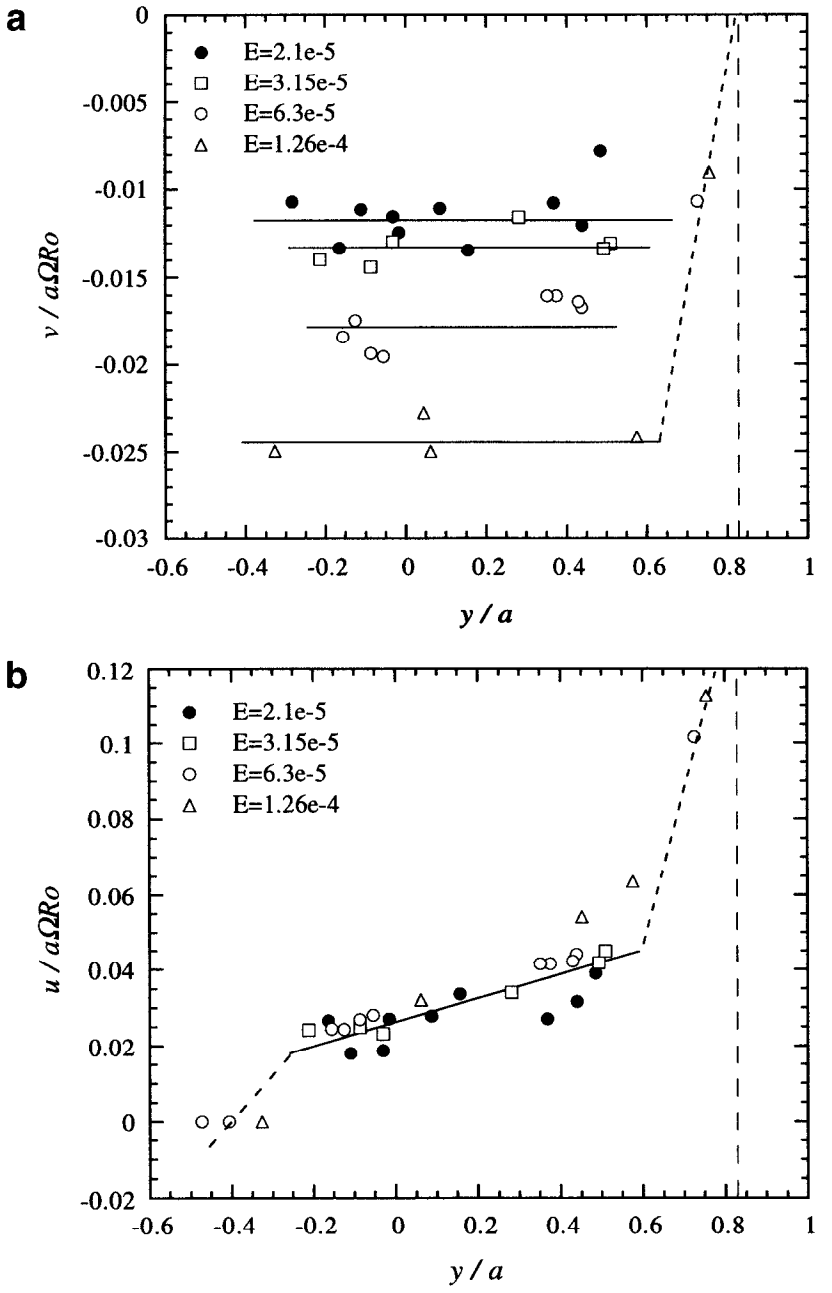

Figure 10. Normalized components of the velocity along and across the center line $x = 0$ in the interior as functions of the latitude y/a for four runs with anticyclonic forcing, similar Rossby numbers between 0.01 and 0.02 and various values of E: (a) northward component v, (b) eastward component u. The vertical dashed line indicates the position of the edge of the slope; the solid straight lines are the best fits by linear regression.

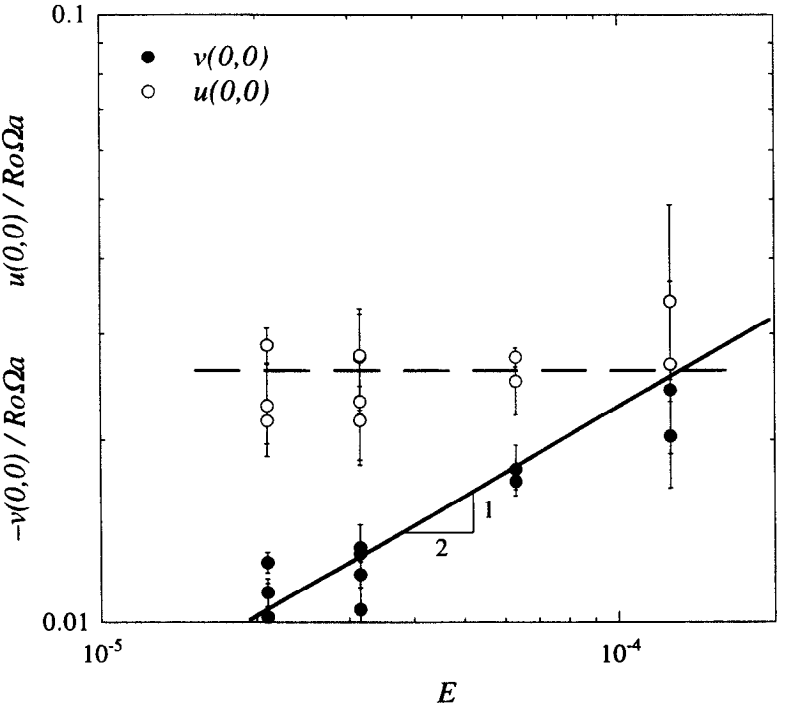

Figure 11. Normalized values of the u (O) and v (●) components of velocity at the center of the basin ($x = 0$, $y = 0$) for each of the runs with anticyclonic forcing, as functions of the Ekman number. The solid line is the $E^{1/2}$-power law curve of best fit.

case. The column enters the slope region at the northwest and is carried around on a circle of constant depth until it gets near its point of origin. However, its depth is less than the depth that it had to begin with. In order to get to its original starting point the column must cross depth contours toward deeper water. As it does so, it loses the potential vorticity that it gained from the wind. For the linear case, essentially all of the frictional dissipation takes place in the region where the column crosses depth contours so friction restores the column to its point of origin not along the western boundary as it does in Stommel's model, but on the eastern side where the cross-contour flow takes place. Of course, crossing of depth contours in the present configuration is equivalent to crossing lines of latitude in the oceanic case.

The enormous difference between the flows with cyclonic and anticyclonic forcing can be qualitatively understood as follows. For cyclonic forcing a column of fluid enters the interior on the eastern side and is driven northward by the rotating lid. As the Rossby number is increased, inertia forces the column to shoot past the linear exit point but the column is moving meridionally in the direction required by the forcing. Inertia also increases the westward zonal flow and the net effect is a trajectory that is more zonal than it

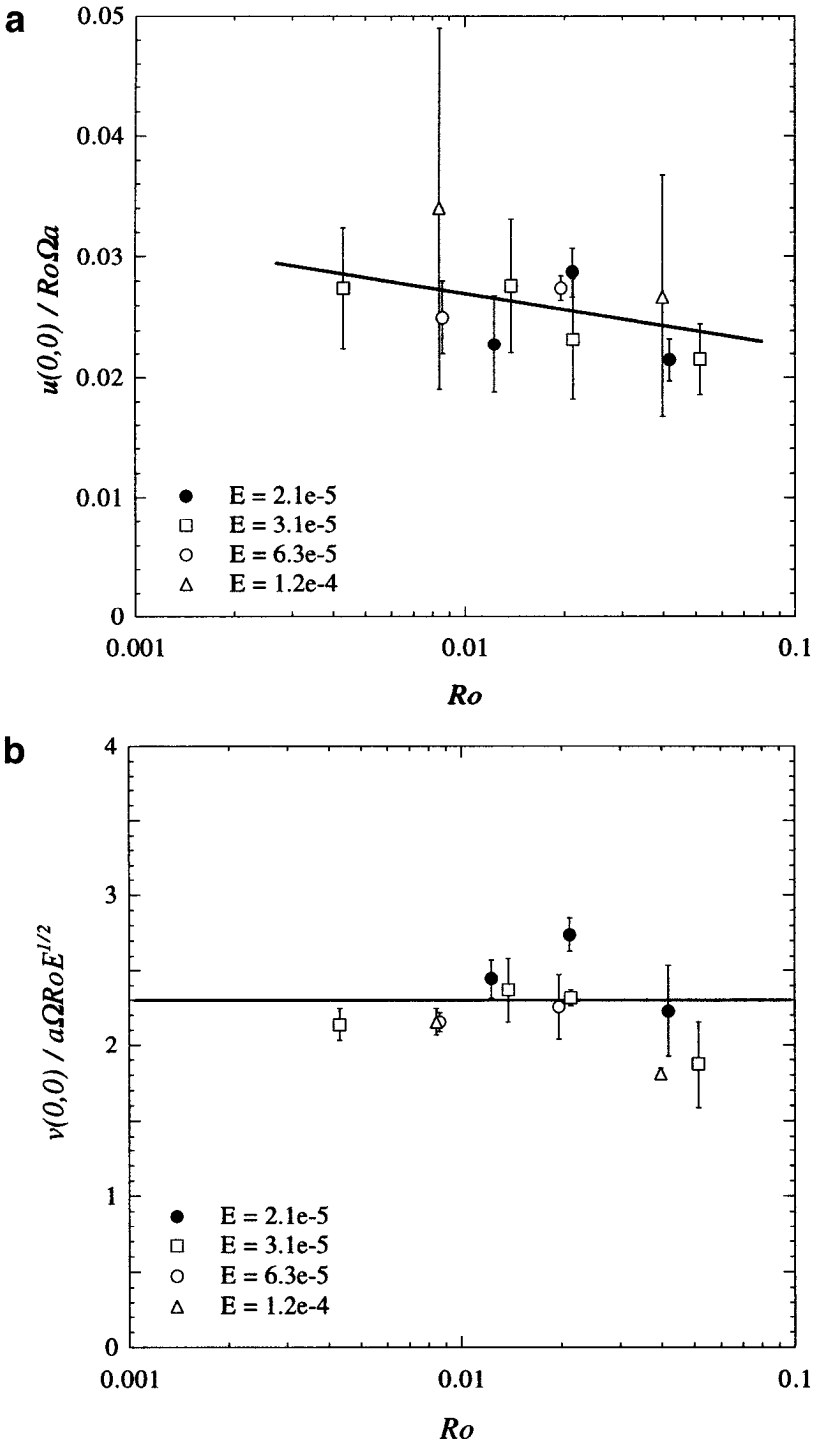

Figure 12. Normalized values of (a) the eastward velocity u and (b) the northward velocity v at the center of the tank in runs with anticyclonic forcing as functions of the Rossby number. In (b) the normalization of v utilizes the $E^{1/2}$-dependence from Figure 11. Data symbols indicate the Ekman number and the straight lines are from linear regressions.

is in the linear case. Thus, inertia gives rise to a pattern of streamlines that is flatter (more zonal) than, but qualitatively very similar to, the linear pattern.

With anticyclonic driving a column of fluid in the linear case leaves the slope region in the northwest and turns and flows southwestward toward the point where it re-enters the slope region. With increased Rossby number the column shoots past the linear exit point in the northwest and flows northward in the interior. Thus, the meridional component of velocity is in the direction opposite to the direction required by the forcing. Hence, the column must make a loop and return southward to a point where the southward forcing of the lid can deliver it to the southeastern side where it enters the slope region. But inertia carries the column beyond its equilibrium point so it must turn northward again. Thus, an oscillation is generated and the looping motion can create eddies, first an anticyclonic eddy and then on the second overshoot a cyclonic eddy.

An additional difference is that inertial effects are large in the southeast for cyclonic driving and large in the northwest for anticyclonic driving. By the argument above, inertia in the southeast simply alters the cyclonic pattern slightly. The extra (Ekman) friction in the interior helps the fluid to adjust to the mildly altered pattern. But in the anticyclonic case the strong looping motions in the northwest cause dissipation of negative vorticity in the anticyclonic loop and dissipation of positive vorticity in the cyclonic loop. When viscosity is high and nonlinear effects not too large, mainly negative vorticity is dissipated and the flow quickly settles down to the southeastward drift of the interior. With smaller friction a positive eddy forms on the offshore side of the big anticyclonic eddy (one such can be seen about 30° north of west in Figure 6a iv) and the flow in the northwest becomes transient with substantial dissipation taking place throughout the region. Thus, dissipation is divided between the southeastern part of the basin where the interior flow enters the slope region and crosses depth contours, just as it does in the linear system, and the northwest where dissipation accompanies the transient flow.

How much dissipation takes place in each region cannot be determined without a numerical calculation of the nonlinear system. In the cyclonic case dissipation seems to be predominantly near the region where the flow crosses depth contours, although for strongly nonlinear flow there is an indication of some dissipation where the interior flow joins the slope region in the northwest. Whatever the actual distribution of dissipation is in the two cases, it is certainly different from the traditional picture of frictional effects concentrated in the western boundary layer. Thus, a much more thorough study of the distribution of dissipation in basins with topography is needed to determine just where the vorticity injected by the wind is dissipated.

Acknowledgments. We are indebted to Derrick Corrigan, who put together the tank with the sloping bottom, to Rick Salmon and Louis Howard for discussions during the course of the work and to the National Science Foundation for support through grant OCE 9312523. This article is dedicated to the memory of Pierre Welander, who carried out some of the first investigations of circulation with topography. Those of us who knew him remember a man of great originality and a series of interactions that still keeps us smiling.

REFERENCES

Beardsley, R. C. 1969. A laboratory model of the wind-driven ocean circulation. J. Fluid Mech., *38,* 255–271.

—— 1973. A numerical model of the wind-driven ocean circulation in a circular basin. Geophys. Fluid Dyn., *4,* 211–241.

—— 1975. The 'sliced-cylinder' laboratory model of the wind-driven ocean circulation. Part 2. Oscillatory forcing and Rossby wave resonance. J. Fluid Mech., *69,* 41–64.

Beardsley, R. C. and K. Robbins. 1975. The 'sliced-cylinder' laboratory model of the wind-driven ocean circulation. Part 1. Steady forcing and topographic Rossby wave instability. J. Fluid Mech., *69,* 27–40.

Becker, A. and M. A. Page. 1990. Flow separation and unsteadiness in a rotating sliced cylinder. Geophys. Astrophys. Fluid Dyn., *55,* 89–115.

Becker, J. M. and Rick Salmon. 1997. Eddy formation on a continental slope. J. Mar. Res., *55,* 181–200.

Dengg, J. 1993. The problem of Gulf Stream separation: a barotropic approach. J. Phys. Oceanogr., *23,* 2183–2200.

Griffiths, R. W. and P. Cornillon. 1994. Laboratory experiments with mid-latitude circulation in a two-layer ocean, *in* Proc. 4th Internat. Symp. on Stratified Flows, Grenoble, E. Hopfinger, B. Voisin and G. Chavand, eds.

Griffiths, R. W. and A. E. Kiss. 1997. Flow regimes in a wide 'sliced-cylinder' model of homogeneous ocean circulation. J. Fluid Mech. (submitted).

Haidvogel, D. B., J. C. McWilliams and P. R. Gent. 1992. Boundary current separation in a quasigeostrophic, eddy-resolving ocean circulation model. J. Phys. Oceanogr., *22,* 882–902.

Kamenkovich, V. M., V. A. Sheremet, A. R. Pastushkov and S. O. Belotserkovsky 1995. Analysis of the barotropic subtropical gyre in the ocean for finite Reynolds numbers. Part I. J. Mar. Res., *53,* 959–994.

Munk, W. H. 1950. On the wind-driven ocean circulation. J. Meteor., *7,* 79–93.

Pedlosky, J. and H. P. Greenspan. 1967. A simple laboratory model for the oceanic circulation. J. Fluid Mech., *27,* 291–304.

Salmon, Rick. 1992. A two-layer Gulf Stream over a continental slope. J. Mar. Res., *50,* 341–365.

Stommel, H. 1948. The westward intensification of wind-driven ocean currents. Trans. Am. Geophys. Union, *29,* 202.

Received: *19 August 1997;* revised: *18 September, 1997.*